ACS APPLIED MATERIALS & INTERFACES

Research Article

www.acsami.org

# Carbon Quantum Dot-Based Field-Effect Transistors and Their Ligand Length-Dependent Carrier Mobility

Woosung Kwon, Sungan Do, Dong Chan Won, and Shi-Woo Rhee*

System on Chip Chemical Process Research Center, Department of Chemical Engineering, Pohang University of Science and Technology (POSTECH), Pohang 790-784, South Korea

**ABSTRACT:** We report electrical measurements of films of carbon quantum dots (CQDs) that serve as the channels of field-effects transistors (FETs). To investigate the dependence of the field-effect mobility on ligand length, colloidal CQDs are synthesized and ligand-exchanged with several primary amines of different ligand lengths. We measure current as a function of gate voltage and find that the devices show ambipolar conductivity, with electron and hole mobilities as high as $8.49 \times 10^{-5}$ and $3.88 \times 10^{-5}$ $cm^2$ $V^{-1}$ $s^{-1}$, respectively. The electron mobilities are consistently 2−4 times larger than the hole mobilities. Furthermore, the mobilities decrease exponentially with the increase of the ligand length, which is well-described by the Miller−Abrahams model for nearest-neighbor hopping. Our results provide a theoretical basis to examine charge transport in CQD films and offer new prospects for the fabrication of high-mobility CQD-based optoelectronic devices, including solar cells, light-emitting devices, and optical sensors.

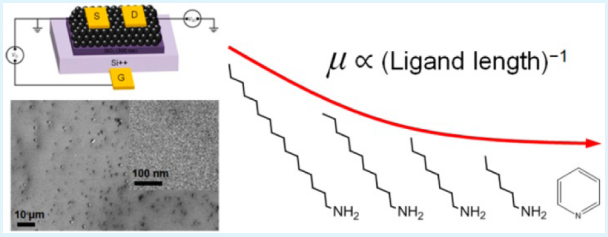


**KEYWORDS:** *carbon quantum dots, mobility, ligand exchange, ligand length, emulsion template, field-effect transistors*

## INTRODUCTION

Carbon quantum dots (CQDs) are emerging as viable candidates for conventional inorganic nanocrystals, because of their low cost, low toxicity, long-term stability, and bright luminescence.[1] Many groups report various routes to derive CQDs, including arc discharge,[2] laser ablation,[3−6] electrochemical oxidation,[7−10] thermal oxidation,[11−15] silica-supported,[16,17] microwave,[18,19] hydrothermal,[20,21] hot injection,[22] unzipping,[23] and emulsion-assisted methods.[24,25] The common structure of CQDs is defined as the quasi-spherical graphitic nanoparticle with various types of surface functional groups (e.g., aldehydes, carboxylic acids, hydroxides, etc.).

The surface of CQDs are often passivated (or "capped") by organic compounds to improve the luminescence quality. These organic compounds, so-called "ligands", have reactive heads (or "anchors") and nonreactive tails. A ligand could bind to CQDs via chemical bonding between the ligand head and the surface functional group. The ligand tail is generally bulky (e.g., long carbon chains, polymers, etc.), which can effectively inhibit the aggregation between CQDs.

In the electrical aspect, ligands form an insulating shell to retard charge transport in nanoparticle films. Experimental studies of charge transport in inorganic nanocrystal films (e.g., PbSe solids, etc.) have revealed that carrier mobility increases exponentially with the decrease of ligand length.[26−30] Thus, in this field, a ligand exchange from shorter to longer molecules has been widely applied to improve the mobility. On the other side, charge transport mechanism in CQD films still remains obscure to impose limitations on their practical application in optoelectronic devices. For instance, Liu and Ma groups recently reported CQD-based light-emitting devices, but the operation voltage is quite high (ca. 9 V), because of the presence of insulating ligands.[31] Thus, it is an urgent matter to develop a ligand exchange technique for CQDs and study the charge-transport mechanism in CQD films for their future applications.

In this work, for the first time, we report on charge transport in films of amine-capped CQDs that serve as the channels of field-effect transistors. Colloidal CQDs are synthesized according to a modified version of the micelle-assisted method. To demonstrate the effect of ligand length on charge transport, the as-synthesized CQDs are ligand exchanged with several shorter-tailed primary amines. Progress of the ligand exchange is traced by measuring absorbance of the sample. We measure current as a function of the gate voltage and find that the devices show ambipolar conductivity with larger electron mobilities. Our results are consistent with previous studies of inorganic nanocrystal films and are well-described by the nearest-neighbor hopping mechanism.

## EXPERIMENTAL SECTION

**Synthesis of Hexadecylamine-Capped CQDs.** All chemicals were purchased from Sigma−Aldrich and used as-received, unless otherwise specified. Synthesis of the hexadecylamine (HDA)-capped CQDs was carried out as described in ref 25 (the micelle-assisted method), with slight modification. Bis(2-ethylhexyl) sulfosuccinate sodium salt (AOT) was dried at 90 °C under argon for 3 h prior to use. Glucose (0.108 g, 10 wt %) in distilled water (1.08 mL) was added to a solution of AOT (880 mg, 0.1 mol) in decane (20 mL), which

Received: October 19, 2012
Accepted: January 16, 2013
Published: January 16, 2013

  

gave a water/AOT molar ratio of 30. The milky solution became transparent within a few seconds, under vigorous stirring, which indicates the formation of the water-in-oil reverse micelles. The reaction flask was then flushed by argon and the solution was aged at room temperature. After 3 h, HDA was added (1.44 g, 0.3 mol, excess) to the solution and the temperature was increased to 160 °C under argon for 1 h. The resulting dark-brown-colored colloidal suspension of the CQDs was precipitated and rinsed with methanol three times to remove excess reactants. The product was then redispersed in octane (5 mg $mL^{-1}$) for further use.

**Ligand Exchange.** The purified HDA-capped CQDs were ligand-exchanged with several short-tailed primary amines, including dodecylamine, octylamine, hexylamine, and pyridine. Ligand exchange was carried out by adding the HDA-capped CQDs to the liquid of one of the modifying ligands under vigorous stirring and moderate heating (80 °C) for 24 h. The ligand-exchanged CQDs were subsequently incubated for another 24 h. The product was rinsed with methanol, separated by centrifugation, and redispersed in octane (5 mg $mL^{-1}$).

**Characterization and Spectroscopic Measurements.** Infrared spectra (IR) were obtained using a Nicolet Model 6700 FT-IR spectrometer. The samples were introduced in demountable KBr cells with a cell holder (Pike Technologies) for IR analysis. For transmission electron microscope (TEM) measurements, a drop of the sample suspension in octane was placed on a copper grid (300 mesh, Electron Microscopy Sciences) and coated with a carbon film, and then the grid was vacuum-dried. TEM images were obtained using a Jeol Model JEM-2200FS system with the image Cs-corrector at an accelerating voltage of 200 kV. UV−visible absorption spectra were recorded on a Mecasys Optizen POP spectrophotometer. Photoluminescence spectra were recorded on a Jasco Model FP-6500 fluorometer. For quantum yield measurements, a solution of quinine sulfate in 0.1 M $H_2SO_4$ (the literature quantum yield of 54% at 360 nm) was used as a standard. The quantum yield can be calculated using the following equation:

$$Q = Q_S\left(\frac{I}{I_S}\right)\left(\frac{F_S}{F}\right)\left(\frac{n}{n_S}\right)^2 \quad (1)$$

where $Q$ is the quantum yield, $I$ the integrated area under the emission spectrum, $F$ the absorbance at the excitation wavelength ($F = 1 - 10^{-D}$, where $D$ is the optical density), and $n$ the refractive index of the solvent. In all cases, the subscript "S" denotes the standard value. The 10-mm cuvettes were prestored under the excitation wavelength in order to minimize reabsorption.

**Field-Effect Transistor (FET) Measurements.** Prior to the fabrication of the field-effect transistors (FETs), $p$-doped $Si/SiO_2$ (300 nm) wafers were cut into 2 cm × 2 cm pieces and cleaned in a piranha solution (3:1 v/v $H_2SO_4$:$H_2O_2$). One of the ligand-exchanged CQD suspensions was then spin-cast at 2000 rpm for 30 s onto the cleaned $Si/SiO_2$ substrate. After dried, the film was washed with anhydrous methanol to remove residuals. Repeating these steps more than 20 times gave a uniform film across several square centimeters with a thickness of ca. 100 nm. The resulting CQD film was dried in a vacuum oven at 80 °C overnight. Gold source and drain electrodes (100 nm thickness) were thermally evaporated through a shadow mask onto the film. The channel length and width were 150 and 1500 $\mu$m, respectively. Transfer characteristics of the CQD FETs were obtained using an Agilent Model E5270A Precision Semiconductor Parameter Analyzer under ambient conditions.

## RESULTS AND DISCUSSION

The HDA-capped CQDs (HDA-CQDs) have been prepared via the carbonization of glucose templated by water-in-oil reverse micelles. The reverse micelles containing glucose are formed by mixing a glucose solution (water phase) and decane (oil phase) in the presence of AOT (surfactant). Once the micelles reach a critical supersaturation condition by raising the temperature, carbonization is spurred by intermolecular dehydration of glucose. The growth is terminated when HDA ligands chemically bind to the surface. Figure 1 shows infrared spectra of glucose and the HDA-CQDs, respectively. The

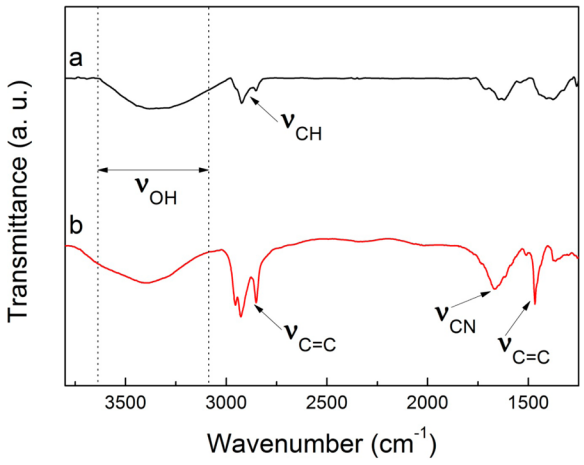


**Figure 1.** Infrared spectra of (a) glucose and (b) the HDA-CQDs. Several peaks discussed in the text are indicated by the arrows.

formation of the graphitic core structure is confirmed by the peaks near 1500 and 3000 $cm^{-1}$ designated to the vibrational stretching of C═C. The evolution of the broad amide peak near 1600 $cm^{-1}$ indicates that HDA ligands successfully bind to the surface to form amide groups.

Figure 2 shows that the resulting CQDs have a mean diameter of 3.67 nm with a standard deviation of 0.68 nm, as determined by high-resolution transmission electron microscopy (HR-TEM). This uniform dispersion (without any size selection procedure) arises from the nature of reverse micelles which effectively isolate precursors from the bulk phase to prohibit undesirable aggregation. In Figures 2b and 2c, we find that the lattice spacings are 0.23 and 0.34 nm, corresponding to the (100) and (002) facet of graphite, respectively. The fast Fourier transform (see the inset in Figure 2b) reveals a characteristic hexagonal diffraction pattern of the (100) facet of graphite, which further proves the formation of the graphitic structure.

In Figure 3, the HDA-CQDs exhibit typical absorption and emission spectra of fluorescent carbon nanomaterials reported previously.[2−25] The absorption spectrum involves a characteristic shoulder in the UV region (~325 nm) attributed to the presence of aromatic $\pi$-orbitals. Poor absorbance in the visible region (above 550 nm) can be also indicated as one of several spectral features of typical CQDs. The peak position of the emission spectra is dependent on the excitation wavelength, which would be ascribed to emissive surface sites with various energy levels.[22−25] The peak intensity generally decreases as the excitation wavelength increases and, accordingly, the absorbance decreases. We find that the quantum yield of the HDA-CQDs measured at 360 nm excitation is as high as 33%.

Figure 4 shows the spectral properties of the ligand-exchanged CQDs. The modifying ligands share the same anchor group (amine) and differ from each other in their ligand lengths. In Figure 4a, the ligand-exchanged CQDs with dodecylamine (DDA), octylamine (OA), and hexylamine (HA) preserve several features of the absorption and emission spectra of the original HDA-CQDs. They commonly exhibit absorbance shoulders and decays in the UV and visible regions, respectively. The excitation wavelength-dependent emission spectra are also found and their peak positions are consistent


dx.doi.org/10.1021/am3023898 | ACS Appl. Mater. Interfaces 2013, 5, 822−827

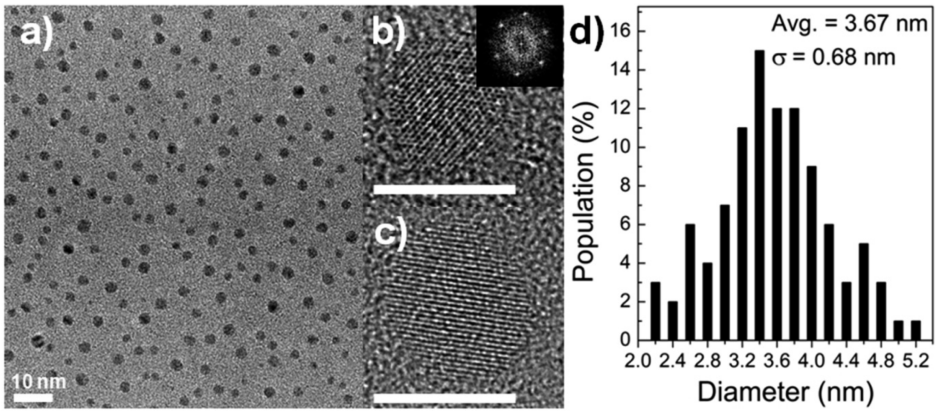


**Figure 2.** (a,b,c) HR-TEM images and (d) population statistics of the HDA-CQDs (mean diameter = 3.67 nm and standard deviation = 0.68 nm). A low-magnification TEM image was used for the population statistics ($N \approx 1000$). The scale bars in panels (b) and (c) indicate 3 nm. The inset in panel (b) shows the fast-Fourier-transformed diffraction pattern.

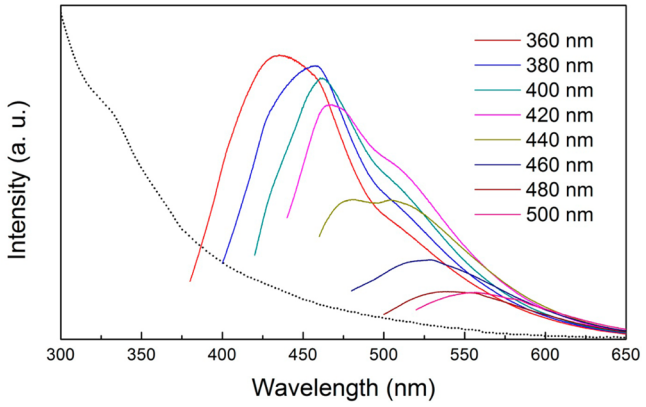


**Figure 3.** Absorption (black dotted line) and emission (colored solid lines) spectra of the HDA-capped CQDs. The color coding represents the excitation wavelength.

with those of the HDA-CQDs. This can be attributed to the fact that HDA, DDA, OA, and HA share the chemical similarity (primary alkyl amines). On the other hand, the ligand-exchanged CQDs with pyridine (PRD) are distinguishable by their absorption spectrum involving two characteristic peaks in the UV region. The origin of these peaks can be indicated that the phenyl groups donated by the PRD ligand are sensitive to the UV light at 257 and 280 nm. To verify the role of the PRD ligand, we have prepared a series of samples incubated for different periods of time. The absorption peak intensity increases as a function of the incubation time, which indicates gradual adsorption of PRD ligands (Figure 4b). It turns out that the ligand exchange rate exponentially decays as a function of the incubation time and the reaction reaches its equilibrium after 12 h (Figure 4c). This result, in fact, was used to deduce the incubation time required for the other ligand exchange reactions (DDA, OA, and HA), because the progress can be hardly traced due to their chemical similarity.

To investigate the effect of the ligand length on long-range charge transport, CQD-based field effect transistors (CQD FETs) have been fabricated by means of layer-by-layer spin-casting. Figure 5 shows the transfer characteristics of a series of the CQD FETs with ambipolar conductivity. The drain current ($I_D$) of the CQD FETs increases as the ligand length decreases; finally, the PRD-CQD FETs show a 100-fold larger $I_D$ value than the HDA-CQD FETs in the saturation regime (see Figure 5b).

In Figure 5c, the asymmetric V-shape in the linear regime of source-drain bias ($V_{SD}$) implies unequal electron and hole mobilities, where the positive and negative slopes ($\partial I_D/\partial V_G$) of each curve indicate the electron and hole transport, respectively. From the data shown in Figure 5c, electron and hole mobilities ($\mu$) can be extracted by the gradual channel approximation

$$\frac{\partial I_D}{\partial V_G} = \frac{WC_{ox}}{L} V_{SD}\mu \tag{2}$$

where $V_G$ is the gate voltage, $W$ the channel width, $L$ the channel length, and $C_{ox}$ the dielectric capacitance per unit area (10 nF cm$^{-2}$ for 300-nm-thick $SiO_2$). The left-hand side of eq 2 can be estimated by a linear fit of each $I_D-V_G$ curve. Finally, we find that the electron mobilities are consistently 2−4 times larger than the hole mobilities (Table 1). This observation coincides with previous studies of chemically treated PbSe FETs and can be attributed to a higher density of states for electrons.[28,30,32,33] The highest electron and hole mobilities were recorded with the PRD-CQD FETs (the shortest ligand length), which are more than 100 times greater than the lowest electron and hole mobilities of the HDA-CQD FETs (the longest ligand length). Previous studies of PbSe FETs report mobilities of $10^{-4}-10^{-2}$ cm$^2$ V$^{-1}$ s$^{-1}$, which are 1−3 orders of magnitude larger than our best record.[30] We find that smaller mobilities are most likely, because the CQDs have a lower density of states for charge carriers than for inorganic nanocrystals.

We assume that charge transport in CQD films is achieved by a series of nearest-neighbor hopping or incoherent tunneling transitions between adjacent CQDs. Since the rate of tunneling transitions is a function of the width and the height of tunnel barriers, the mobility of charge carriers in randomly distributed CQD films can be expressed as a product of exponents of those two variables (the Miller−Abrahams approximation):[30]

$$\mu = \mu_0 \exp(-0.865\beta d) \exp\left(-\frac{\Delta E}{kT}\right) \tag{3}$$

where $\beta$ is the tunneling decay constant, $d$ the (average) barrier width, $\Delta E$ the (average) barrier height, and $T$ the temperature. At high $V_{SD}$, the activation energy for conduction is given by


dx.doi.org/10.1021/am3023898 | ACS Appl. Mater. Interfaces 2013, 5, 822−827

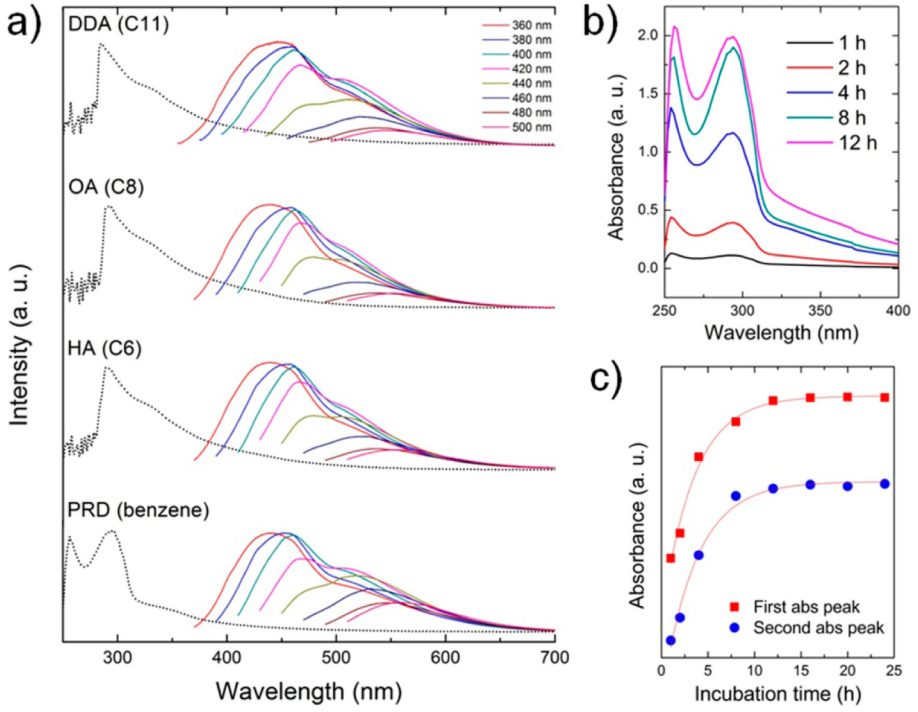


**Figure 4.** (a) Absorption (black dotted line) and emission spectra (colored solid lines) of the ligand-exchanged CQDs. The color coding represents the excitation wavelength and is the same for all graphs. (b) Absorption spectra of the PRD-CQDs incubated for different periods of time. The samples incubated more than 12 h show almost the same absorption spectra so that excluded. (c) The absorption peak intensity as a function of the incubation time. The red lines are exponential fits to the data. The sample concentration is fixed at 0.1 mg $mL^{-1}$ in this experiment.

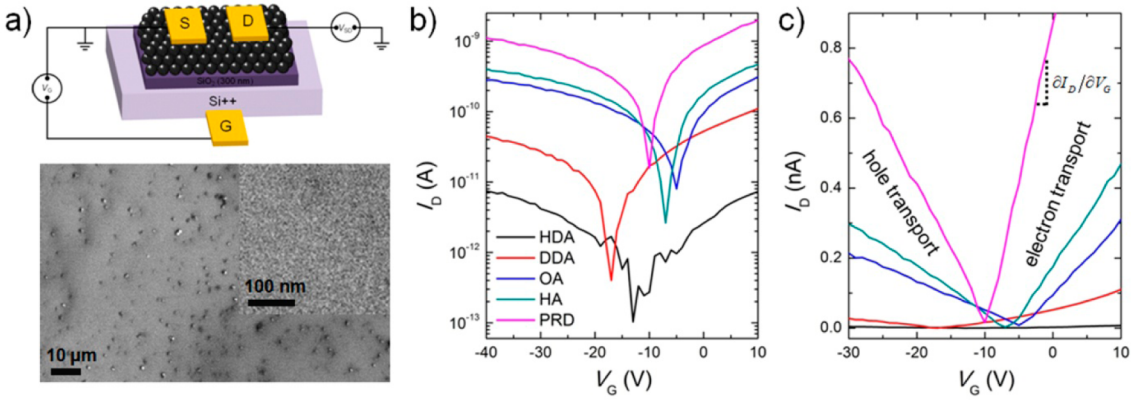


**Figure 5.** (a) Schematic of the FET and SEM images of the CQD channel (HA-CQD). Transfer characteristics of a series of the CQD FETs on (b) semilogarithmic and (c) linear plots at $V_{SD} = -30$ V. The channel length and width are 150 and 1500 $\mu$m, respectively. The color coding is the same for both graphs.

**Table 1. Electron and Hole Mobilities of a Series of the CQD FETs Extracted from Figure 5c**

| | mobility ($cm^2$ $V^{-1}$ $s^{-1}$) | |
|---|---|---|
| ligand | electron | hole |
| HDA | $9.91 \times 10^{-7}$ | $4.78 \times 10^{-7}$ |
| DDA | $4.46 \times 10^{-6}$ | $2.22 \times 10^{-6}$ |
| OA | $1.12 \times 10^{-5}$ | $5.52 \times 10^{-6}$ |
| HA | $2.76 \times 10^{-5}$ | $9.11 \times 10^{-6}$ |
| PRD | $8.49 \times 10^{-5}$ | $3.88 \times 10^{-5}$ |

only the energy required to generate electrons or holes ($\beta$ and $\Delta E$ are neglected).[34]

Here, we chose $V_{SD} = -30$ V, smaller than $kT$ to minimize the effect of the external field on the charge transport. We assume that the last exponential term is constant at room temperature ($kT > \Delta E$). Then, eq 3 indicates that the mobility decreases exponentially with the increase of the barrier width.

We display the mobilities in Table 1 as a function of the ligand length on a semilogarithmic plot (Figure 6). As noted, in connection with eq 3, the data fit well to a linear equation,

$$\ln \mu = Ad + B$$

with $A = \ln \mu_0$ and $B = -0.865\beta$. This observation allows us to extract the tunneling decay constants for electrons ($\beta_e$) and holes ($\beta_h$) of 0.303 and 0.291 Å, respectively. These values are consistent with previous studies of tunneling transitions in alkane(di)thiol self-assembled monolayers and inorganic nanocrystal films.[30,35−37] We note that the alkanethiol-mediated tunneling transitions have $\beta$ values that are ~2 times larger than


dx.doi.org/10.1021/am3023898 | ACS Appl. Mater. Interfaces 2013, 5, 822−827

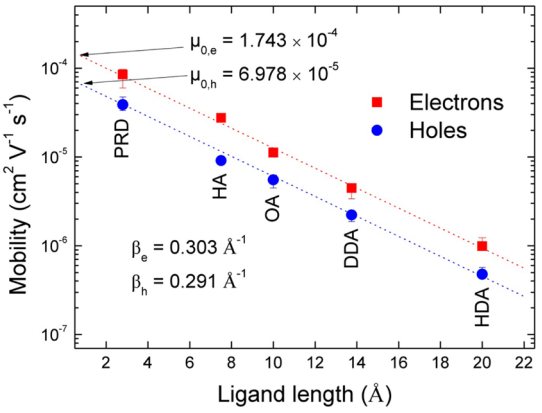


**Figure 6.** Mobility versus ligand length with $V_{SD}$ = −10 V in a series of the CQD FETs. We assume 1.25 Å per C−C (or C−N) bond and that the barrier width is proportional to the ligand length.[40] The error bars show the spread in data from 10 samples. The dotted lines are linear fits to the data.

our results (alkylamine). This can be attributed to the fact that N atoms have much smaller orbitals than S atoms. From the WKB approximation,

$$\beta = \sqrt{\frac{2m^* \Delta E}{\hbar^2}}$$

where $m^*$ is the effective mass, we find $\Delta E \approx 1.0$ eV with $m^* = 0.28m_e$ for tunneling transitions via the aliphatic ligand.[38] The similar $\beta_e$ and $\beta_h$ values imply that the barrier heights for electrons and holes are almost identical. Thus, we conclude that the larger electron mobility stems from a higher density of states for electrons associated with the larger $\mu_0$. The N atoms on the surface (from the amine ligands) may provide the additional energy states for electrons.[39]

## CONCLUSIONS

In summary, we have synthesized a series of the ligand-exchanged carbon quantum dots (CQDs), and we have shown that our CQD field-effect transistors (FETs) are well-described by the nearest-neighbor hopping model. By modulating the gate voltage, we find that the CQD FETs show ambipolar transport with electron and hole mobilities as high as 8.49 × $10^{-5}$ and 3.88 × $10^{-5}$ cm$^2$ V$^{-1}$ s$^{-1}$, respectively. The electron mobilities are consistently 2−4 times larger than the hole mobilities, because of a larger density of states for electrons. The mobilities decrease exponentially as the ligand length (the barrier width) increases, which is consistent with the Miller−Abrahams approximation for nearest-neighbor hopping. Further investigation of the dependence of current in CQD FETs on other variables (temperature, size, surface functional groups, etc.,) is required to reveal the origin of charge carriers for ambipolar conduction. We expect that our results will stimulate theoretical studies of the electrical property of CQD films and also their wide application in optoelectronic devices, including optical sensors, solar cells, and light-emitting devices.

## AUTHOR INFORMATION

### Corresponding Author

*Tel.: 82-54-279-2265. Fax: 82-54-279-8619. E-mail: srhee@postech.ac.kr.

### Notes

The authors declare no competing financial interest.

## ACKNOWLEDGMENTS

This research was supported by the Korea Research Foundation (KRF) through the National Research Laboratory Project and POSCO Research Program for Fusion Technology of Materials. The authors thank Hyun-Jin Park (NCNT) for his technical assistance in the TEM analysis. W.K. is grateful to Eun Ji Goh and Hyemin Kim for valuable discussions.

## REFERENCES

(1) Baker, S. N.; Baker, G. A. *Angew. Chem., Int. Ed.* **2010**, *49*, 6726−6744.
(2) Xu, X. Y.; Ray, R.; Gu, Y. L.; Ploehn, H. J.; Gearheart, L.; Raker, K.; Scrivens, W. A. *J. Am. Chem. Soc.* **2004**, *126*, 12736−12737.
(3) Cao, L.; Wang, X.; Meziani, M. J.; Lu, F. S.; Wang, H. F.; Luo, P. J. G.; Lin, Y.; Harruff, B. A.; Veca, L. M.; Murray, D.; Xie, S. Y.; Sun, Y. P. *J. Am. Chem. Soc.* **2007**, *129*, 11318−11319.
(4) Hu, S. L.; Niu, K. Y.; Sun, J.; Yang, J.; Zhao, N. Q.; Du, X. W. *J. Mater. Chem.* **2009**, *19*, 484−488.
(5) Sun, Y. P.; Zhou, B.; Lin, Y.; Wang, W.; Fernando, K. A. S.; Pathak, P.; Meziani, M. J.; Harruff, B. A.; Wang, X.; Wang, H. F.; Luo, P. J. G.; Yang, H.; Kose, M. E.; Chen, B. L.; Veca, L. M.; Xie, S. Y. *J. Am. Chem. Soc.* **2006**, *128*, 7756−7757.
(6) Wang, X.; Cao, L.; Lu, F. S.; Meziani, M. J.; Li, H.; Qi, G.; Zhou, B.; Harruff, B. A.; Kermarrec, F.; Sun, Y. P. *Chem. Commun.* **2009**, 3774−3776.
(7) Zheng, L. Y.; Chi, Y. W.; Dong, Y. Q.; Lin, J. P.; Wang, B. B. *J. Am. Chem. Soc.* **2009**, *131*, 4564−4565.
(8) Zhao, Q. L.; Zhang, Z. L.; Huang, B. H.; Peng, J.; Zhang, M.; Pang, D. W. *Chem. Commun.* **2008**, 5116−5118.
(9) Lu, J.; Yang, J.-X.; Wang, J.; Lim, A.; Wang, S.; Loh, K. P. *ACS Nano* **2009**, *3*, 2367−2375.
(10) Li, H.; He, X.; Kang, Z.; Huang, H.; Liu, Y.; Liu, J.; Lian, S.; Tsang, C. H. A.; Yang, X.; Lee, S.-T. *Angew. Chem., Int. Ed.* **2010**, *49*, 4430−4434.
(11) Bottini, M.; Mustelin, T. *Nat. Nanotechnol.* **2007**, *2*, 599−600.
(12) Cao, L.; Sahu, S.; Anikumar, P.; Bunker, C. E.; Xu, J.; Fernando, K. A. S.; Wang, P.; Guliant, E. A.; Tackett, K. N.; Sun, Y.-P. *J. Am. Chem. Soc.* **2011**, *133*, 4754−4757.
(13) Liu, H.; Ye, T.; Mao, C. *Angew. Chem., Int. Ed.* **2007**, *46*, 6473−6475.
(14) Tian, L.; Ghosh, D.; Chen, W.; Pradhan, S.; Chang, X.; Chen, S. *Chem. Mater.* **2009**, *21*, 2803−2809.
(15) Ray, S. C.; Saha, A.; Jana, N. R.; Sarkar, R. *J. Phys. Chem. C* **2009**, *113*, 18546−18551.
(16) Bourlinos, A. B.; Stassinopoulos, A.; Anglos, D.; Zboril, R.; Georgakilas, V.; Giannelis, E. P. *Chem. Mater.* **2008**, *20*, 4539−4541.
(17) Liu, R. L.; Wu, D. Q.; Liu, S. H.; Koynov, K.; Knoll, W.; Li, Q. *Angew. Chem., Int. Ed.* **2009**, *48*, 4598−4601.
(18) Zhu, H.; Wang, X. L.; Li, Y. L.; Wang, Z. J.; Yang, F.; Yang, X. R. *Chem. Commun.* **2009**, 5118−5120.
(19) Jaiswal, A.; Ghosh, S. S.; Chattopadhyay, A. *Chem. Commun.* **2012**, *48*, 407−409.
(20) He, X.; Li, H.; Liu, Y.; Huang, H.; Kang, Z.; Lee, S.-T. *Colloids Surf. B* **2011**, *87*, 326−332.
(21) Hsu, P.-C.; Chang, H.-T. *Chem. Commun.* **2012**, *48*, 3984−3986.
(22) Wang, F.; Pang, S.; Wang, L.; Li, Q.; Kreiter, M.; Liu, C.-Y. *Chem. Mater.* **2010**, *22*, 4528−4530.
(23) Guo, X.; Wang, C.-F.; Yu, Z.-Y.; Chen, L.; Chen, S. *Chem. Commun.* **2012**, *48*, 2692−2694.
(24) Kwon, W.; Do, S.; Rhee, S.-W. *RSC Adv.* **2012**, 21122311226.
(25) Kwon, W.; Rhee, S.-W. *Chem. Commun.* **2012**, *48*, 5256−5258.
(26) Markovich, G.; Collier, C. P.; Henrichs, S. E.; Remacle, F.; Levine, R. D.; Heath, J. R. *Acc. Chem. Res.* **1999**, *32*, 415−423.
(27) Vanmaekelbergh, D.; Liljeroth, P. *Chem. Soc. Rev.* **2005**, *34*, 299−312.
(28) Talapin, D. V.; Murray, C. B. *Science* **2005**, *310*, 86−89.
(29) Talapin, D. V.; Lee, J.-S.; Kovalenko, M. V.; Shevchenko, E. V. *Chem. Rev.* **2010**, *110*, 389−458.

(30) Liu, Y.; Gibbs, M.; Puthussery, J.; Gaik, S.; Ihly, R.; Hillhouse, H. W.; Law, M. *Nano Lett.* **2010**, *10*, 1960−1969.
(31) Wang, F.; Chen, Y.; Liu, C.; Ma, D. *Chem. Commun.* **2011**, *47*, 3502−3054.
(32) Wehrenberg, B. L.; Yu, D.; Ma, J.; Guyot-Sionnest, P. *J. Phys. Chem. B* **2005**, *109*, 20192−20199.
(33) Luther, J. M.; Law, M.; Song, Q.; Beard, M. C.; Nozik, A. J. *ACS Nano* **2008**, *2*, 271−280.
(34) Mentzel, T. S.; Porter, V. J.; Geyer, S.; MacLean, K.; Bawendi, M. G.; Kastner, M. A. *Phys. Rev. B* **2008**, *77*, 075316.
(35) Akkerman, H. B.; Naber, R. C. G.; Jongbloed, B.; val Hal, P. A.; Blom, P. W. M.; de Leeuw, D. M.; de Boer, B. *Proc. Natl. Acad. Sci.* **2007**, *104*, 11161−11166.
(36) Malen, J. A.; Doak, P.; Baheti, K.; Tilley, T. D.; Segalman, R. A.; Majumdar, A. *Nano Lett.* **2009**, *9*, 1164−1169.
(37) Remacle, F.; Beverly, K. C.; Heath, J. R.; Levine, R. D. *J. Phys. Chem. B* **2003**, *107*, 13892−13901.
(38) Tomfohr, J. K.; Sankey, O. F. *Phys. Rev. B* **2002**, *65*, 245105.
(39) Kang, M. S.; Lee, J.; Norris, D. J.; Frisbie, C. D. *Nano Lett.* **2009**, *9*, 3848−3852.
(40) Engelkes, V. B.; Beebe, J. M.; Frisbie, C. D. *J. Am. Chem. Soc.* **2004**, *126*, 14287−14296.